Journal of Biomechanics 66 (2018) 145–152

Contents lists available at ScienceDirect

Journal of Biomechanics

journal homepage: www.elsevier.com/locate/jbiomech
www.JBiomech.com

Predictive multiscale computational model of shoe-floor coefficient of friction

Seyed Reza M. Moghaddam, Arjun Acharya, Mark S. Redfern, Kurt E. Beschorner *

Department of Bioengineering, University of Pittsburgh, Benedum Engineering Hall 302, 3700 O'Hara St., Pittsburgh, PA 15261, United States

ARTICLE INFO

Article history:
Accepted 9 November 2017

Keywords:
Slips and falls
Shoe-floor friction
Coefficient of friction
Finite element modeling

ABSTRACT

Understanding the frictional interactions between the shoe and floor during walking is critical to prevention of slips and falls, particularly when contaminants are present. A multiscale finite element model of shoe-floor-contaminant friction was developed that takes into account the surface and material characteristics of the shoe and flooring in microscopic and macroscopic scales. The model calculates shoe-floor coefficient of friction (COF) in boundary lubrication regime where effects of adhesion friction and hydrodynamic pressures are negligible. The validity of model outputs was assessed by comparing model predictions to the experimental results from mechanical COF testing. The multiscale model estimates were linearly related to the experimental results ($p < 0.0001$). The model predicted 73% of variability in experimentally-measured shoe-floor-contaminant COF. The results demonstrate the potential of multiscale finite element modeling in aiding slip-resistant shoe and flooring design and reducing slip and fall injuries.

1. Introduction

Slips and falls are among the primary causes of injuries. According to the Centers for Disease Control and Prevention, falls were the leading cause of non-fatal injuries between 2001 and 2014 and are responsible for an annual financial burden of $180 billion in the United States (Florence et al., 2015a; Florence et al., 2015b). More than 50% of falls are initiated by slipping accidents in occupational settings (Courtney et al., 2001).

Frictional characteristics of the shoe-floor interface impact the likelihood of slips and falls (Beschorner et al., 2016; Burnfield and Powers, 2006; Hanson et al., 1999). The probability of slips has been predicted with the available coefficient of friction (ACOF) and the required coefficient of friction (RCOF) (Beschorner et al., 2016; Burnfield and Powers, 2006; Hanson et al., 1999; Iraqi et al., 2015). RCOF is measured during gait using force plates on dry surfaces (Chang et al., 2011). ACOF is typically measured using a mechanical device that quantifies the ratio of friction to normal forces between the shoe and flooring (Burnfield and Powers, 2006; Chang et al., 2001a; Hanson et al., 1999; Iraqi et al., 2015). Physics-based computational models of frictional behavior of the shoe-floor-lubricant complex have recently been developed to predict ACOF (Beschorner et al., 2009; Moghaddam et al., 2015). These models have advantages in that: 1. they can help explain the underlying friction mechanisms pertinent to shoe-floor friction, and 2. they can be used to predict and optimize ACOF of hypothetical shoe-floor designs (i.e., they can be used as a design tool).

Shoe-floor friction is influenced by microscopic and macroscopic features of the shoe and flooring. Relevant factors affecting ACOF on the microscopic scale include shoe and flooring surface topography, contact pressure, and outsole material properties (Beschorner et al., 2009; Moghaddam, 2013; Moghaddam et al., 2015). Relevant factors on the macroscopic scale include shoe tread design features such as geometry, tread depth, width and orientation (Blanchette and Powers, 2015; Li and Chen, 2004; Li et al., 2006), material hardness (Moghaddam and Beschorner, 2015; Tsai and Powers, 2008), sliding speed and shoe-floor contact angle (Moghaddam and Beschorner, 2016, 2017; Moyer et al., 2006). Physics-based modeling of the shoe-floor interface has the potential to elucidate how these various features contribute to friction mechanisms.

Contaminants, particularly liquids, play an important role in slipping accidents and can impact friction. Fluid can reduce ACOF by either becoming pressurized, causing a separation of the contacting surfaces (hydrodynamic lubrication) or by reducing adhesion friction without causing a separation (boundary lubrication). While some studies have utilized solely hydrodynamic theory to

* Corresponding author.
E-mail address: beschorn@pitt.edu (K.E. Beschorner).

https://doi.org/10.1016/j.jbiomech.2017.11.009
0021-9290/

Nomenclature

A	contact area
A_{Micro}	nominal area in microscopic models
$ACOF$	available coefficient of friction (experimental)
COF	coefficient of friction
COF_{Model}	coefficient of friction predicted by multiscale model
Δ_q	root mean square slope of surface profiles
$F_{Friction}$	macroscopic friction force
$F_{Hysteresis}$	microscopic friction force due to hysteresis
F_{Normal}	normal load in macroscopic models
$f(p)$	piecewise polynomial describing frictional shear stress due to hysteresis as a function of contact pressure
$G(t)$	variation of shear modulus with respect to time
p	contact pressure
R_z	average peak-to-valley distance of surface profiles
σ_f	frictional shear stress due to hysteresis
τ	time constant of exponential decay in shear modulus

explain ACOF of lubricated surfaces (Beschorner et al., 2007; Li and Chen, 2004), research by our group suggests that dangerously low ACOF values can occur even without hydrodynamic effects (Cowap et al., 2015; Moghaddam et al., 2015; Moore et al., 2012; Strobel et al., 2012). Shoes with at least some tread are demonstrated to operate in boundary lubrication (Beschorner et al., 2014; Singh and Beschorner, 2014) suggesting that boundary lubrication is relevant to slipping. In boundary lubrication, hysteresis deformation of the shoe sole material is the major mechanism contributing to friction (Cowap et al., 2015; Moghaddam et al., 2015; Strobel et al., 2012). Hysteresis friction originates from viscoelastic deformation of the surface asperities (Tabor, 1974). Therefore, modeling hysteresis at the shoe-floor interface is relevant to predicting friction on liquid-contaminated surfaces.

An opportunity exists to use finite element modeling to simulate and predict shoe-floor COF. Finite element modeling has been demonstrated to be effective in modeling the impact of microscopic shoe and floor features on COF (Moghaddam et al., 2015). Furthermore, multiscale computational models have been developed for elastomers that take into account surface features in both microscopic and macroscopic levels to determine hysteresis COF (Wagner et al., 2015a; Wagner et al., 2015b). However, multiscale computational methods have not yet been applied to investigate shoe COF. This study addresses this knowledge gap by applying multiscale computational modeling techniques to actual shoe geometries to predict whole shoe-floor COF.

The purpose of this study is to develop and quantify the predictive ability of a multiscale finite element model for shoe-floor COF. The ability of the multiscale computational model as well as each of its components (microscopic and macroscopic) to predict experimental ACOF are assessed to evaluate the validity of the model. The scope of this model is boundary lubrication regime where adhesion and hydrodynamic pressure effects are negligible.

2. Methods

2.1. Multiscale model

A computational model was developed that included a microscopic and macroscopic finite element model. The microscopic model simulated the interaction between shoe and floor surface asperities to predict the frictional shear stress due to hysteresis as a function of contact pressure (Fortunato et al., 2017; Persson, 2013; Persson, 2001). The macroscopic model simulated shoe heel to floor contact to determine the contact pressure distribution across the outsole surface (Fig. 1). Contact pressure values from the macroscopic model were then combined with the microscopic model to predict the hysteresis COF. Explicit finite element software (LS-Dyna® Livermore Software Technology Corporation, Livermore, California, USA) was used for simulations.

2.1.1. Microscopic model

The microscopic model simulated contact between a rough viscoelastic shoe material and a rough rigid floor. A five-term exponentially decaying function was applied to the shoe, which described the time-dependent behavior of the shear modulus ($G(t)$) (Eq. (1)) (Moghaddam et al., 2015). Flooring was modeled as rigid because it is orders of magnitude harder than the shoe (Beschorner, 2008; Moghaddam et al., 2015). Roughness parameters including the peak-to-valley distance roughness (R_z) and root mean square slope (Δ_q), were incorporated into the models that were consistent with shoes and floors tested in the experimental measurements (See Section 2.2). Specifically, the peak-to-valley distance (R_z) was used to define the vertical distance between peak and valley nodes. Root mean square slope (Δ_q) was used to define the slope of the asperities, which affected the spacing between the asperities (Fig. 1. Left) (Moghaddam et al., 2015).

$$G(t) = \sum_{m=1}^{5} G_m e^{-t/\tau_m}, \tau_m = 10^{-(m-1)}\tau_1, \quad (1)$$

Boundary conditions for the microscopic models included: 1. constraints on the translational and the rotational degrees of freedom at the bottom surface of the floor nodes. 2. Constraints on the translational degrees of freedom were applied at the top surface of the shoe nodes. 3. Contact pressure was controlled using the vertical displacement boundary conditions that were applied at the top surface of the shoe nodes; higher contact pressures were achieved by applying more downward vertical displacement. 4. Velocity boundary conditions consistent with experiments (Section 2.2) were applied to the nodes at the top surface of the shoes. The microscopic model geometries were meshed using eight node hexahedral elements. These elements are well suited for simulating extreme deformations of soft materials (Erhart, 2011).

2.1.2. Macroscopic model

Macroscopic models were either created based on non-contact 3D laser scans (FaroArm®, Faro Technologies, Lake Mary, Florida, USA) of the shoes or CAD models developed based on the measured shoe geometries (ANSYS DesignModeler®, ANSYS Inc., Canonsburg, Pennsylvania, USA). For shoes with repeated pattern geometries, CAD models were developed. For shoes with irregular tread patterns, laser scans were collected, processed to repair surface irregularities (Geomagics®, 3D Systems Corporation, Rock Hill, South Carolina, USA), and tread surface texturing was added to the surface based on the texture's shape, size and orientation (ANSYS DesignModeler®). Since viscoelastic effects were accounted for in the microscopic models, a linear elastic material based on durometer readings was used for the shoes in macroscopic models (Section 2.2).

Displacements and rotations of nodes at the bottom surface of the flooring and top surface of the shoe in the macroscopic models

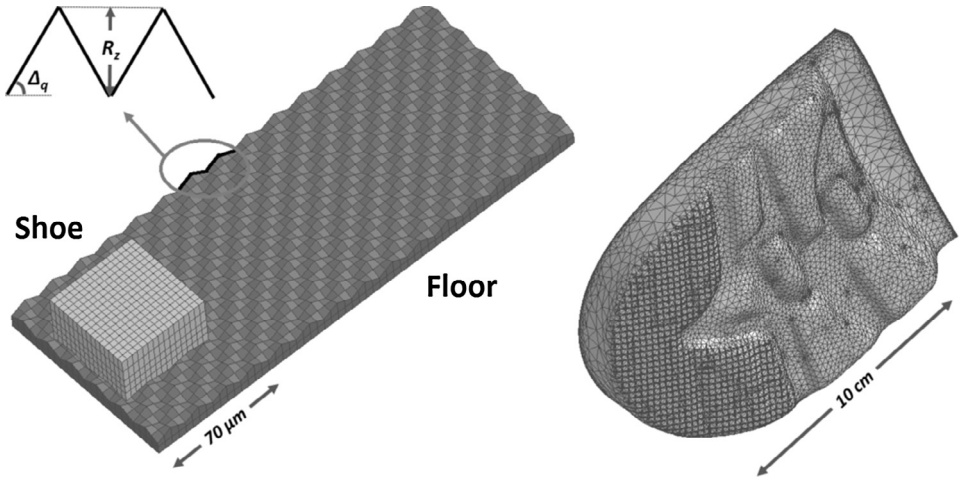

Fig. 1. Representative microscopic (Left. S1-Vinyl) and macroscopic (Right. S6) finite element models. Flooring is not shown in the macroscopic model. A magnified representation of surface asperities is shown in top left corner.

were constrained similar to the microscopic models. The shoe was slid against the flooring at a normal force of 250 N and a horizontal speed of 0.3 m/s. The vertical velocity was 0.3 m/s until the desired vertical force was reached (Section 2.2). Shoe-floor angles consistent with experimental measurements were used in macroscopic models (Section 2.2). Macroscopic models were meshed using tetrahedral elements that are recommended for simulating complex geometries (Erhart, 2011). Flooring was modeled as a rigid material similar to microscopic simulations (Beschorner, 2008; Moghaddam et al., 2015).

2.1.3. Analysis of model data

Frictional shear stress due to hysteresis (σ_f) was calculated as the ratio of the average hysteresis force to the nominal area (Eq. (2)). Average contact pressure in the microscopic models was calculated by dividing the average normal force by the area of the shoe interface in the horizontal plane (i.e., nominal area). Between 16 and 21 contact pressures were evaluated using the model for each shoe-floor combination. A piecewise polynomial fit ($f(p)$) (Wagner et al., 2015b; Wriggers and Reinelt, 2009) was used (MATLAB®, Mathworks, Natick, Massachusetts, USA) to interpolate the shear stress between the discrete levels of contact pressure simulated in microscopic models (Fig. 2 and Eq. (3)). Friction forces for the macroscopic models were calculated based on predicted shear stresses and the areas of contact elements. These friction forces were summed across the contact elements to calculate the net friction force (Eq. (4)). Normal force was calculated based on the contact pressure and the area of elements (Eq. (5)). Whole-shoe COF was the ratio of friction force to normal force (Eq. (6)). A preliminary analysis of the modeling data and experimental data (described in Section 2.2) revealed that the relationship between friction force and normal force was linear with a y-intercept of approximately 0 indicating that this definition of whole-shoe COF is relevant even though Amontons' laws are not broadly applicable to polymers (Hutchings and Shipway, 2017).

$$\sigma_f = \frac{F_{Hysteresis}}{A_{Micro}}, \tag{2}$$

$$\sigma_f(p) = f(p), \tag{3}$$

$$F_{Friction} = \sum f(p_i)A_i, \tag{4}$$

$$F_{Normal} = \sum p_i A_i, \tag{5}$$

$$COF = \frac{F_{Friction}}{F_{Normal}}, \tag{6}$$

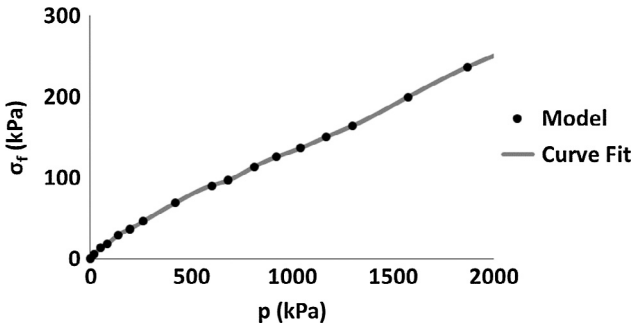

Fig. 2. Representative plot of the frictional shear stress, σ_f, as a function of contact pressure. The gray line indicates the piecewise polynomial curve fit.

2.2. Experimental validation

Model results were compared to experimentally-measured ACOFs for eight different shoes (S1-S8) and two different floorings. Three shoes (work boots) had the same geometry but varying material properties (S6-S8). The remaining five shoes had different tread patterns, material properties and roughness levels (S1-S5). The two floorings included a vinyl composite tile and a high roughness ceramic tile. The high roughness of the ceramic tile was achieved by sand blasting using an aluminum oxide abrasive (Chang et al., 2004; Cowap et al., 2015). Surface characteristics of shoes and floorings were quantified with a stylus profilometer (Taylor-Hobson Surtronic S100®, Leicester, UK). Specifically, roughness parameters were measured with a sampling length of 1.6 mm and a cut-off length of 0.8 mm and averaged across eight measurements at different orientations (Table 1). The ceramic flooring (R_z = 35.6 μm; Δ_q = 35.4°) had a higher roughness than the vinyl flooring (R_z = 9.1 μm; Δ_q = 27.8°) for both parameters.

Shore A hardness of the shoes were characterized using a durometer (Intercomp®, Minneapolis, Minnesota, USA) (ASTM, 2010). Readings were sampled over 2-min at 10 s intervals. Hardness measurements were converted to shear moduli ($G(t)$, Eq. (1)) using methods recommend by Giacomin and Mix (2011) and viscoelastic material models were developed (Table 1, $R^2 > 0.99$ for

Table 1
Roughness and material parameters for modeled shoes.

Shoe	R_z (μm)	Δ_q (°)	G_m (kPa)					
			G_1	G_2	G_3	G_4	G_5	τ_1 (s)
S1	4.03	10.56	1891	40.65	177.6	355.7	0.01772	2041.65
S2	4.81	10.59	2617	46.31	75.77	396	0.2361	1431.02
S3	4.67	11.5	2595	45.15	240	241.7	0.04211	1999.6
S4	7.04	11.87	3764	53.99	17.72	160.5	0.00489	1330.85
S5	6.63	12.61	2989	0.02327	400.3	0	288.5	4450.38
S6	9.35	13.85	2809	95.78	459.4	0.9468	595.9	1663.89
S7	7.99	13.31	5046	583.7	366.9	1.648	235.6	895.26
S8	7.01	13.58	8744	172.5	152.3	0.2857	885.9	1033.38

exponential decay fits). The initial modulus (at $t = 0$, Eq. (1)) was used for modeling the linear elastic shoe material in macroscopic models. Durometer readings were conducted and averaged across nine heel locations for each shoe.

ACOF measurements were performed using a custom-developed robotic slip-tester at a normal force level of 250 N (Aschan et al., 2005; Beschorner et al., 2016; Iraqi et al., 2015); a sliding speed of 0.3 m/s; and shoe-floor angles of 7 ± 2° (ASTM, 2011; Powers and Blanchette, 2014). This speed is within the range of 0–1 m/s that is recommended in literature as 'biofidelic testing' (ASTM, 2011; Chang and Matz, 2001; Powers and Blanchette, 2014). The average ACOF values were calculated for the first 200 ms after reaching a normal force of 250 N (Beschorner et al., 2016; Iraqi et al., 2015). Testing for each shoe-floor combination was repeated over three different days to achieve reliable ACOF values in the presence of potential day to day variability. Five trials were taken for each shoe-floor combination on each day. Shoe-floor angles (Table 2) and sliding speeds were verified using reflective markers placed on the shoes that were tracked using a 14-camera motion capture system (Vicon T40S, Oxford, UK). Canola oil was used as a lubricant in all experiments because preliminary results revealed that this lubricant minimized adhesion forces so that the measured friction was primarily due to hysteresis (Cowap et al., 2015; Goda, 2016; Grosch, 1963; Kluppel and Heinrich, 2000; Menezes and Kailas, 2006; Strobel et al., 2012).

Contact area was measured as an intermediate validation of the macroscopic model. Black ink imprints of shoes on paper (Tencer et al., 2004) were created at the aforementioned angle and force were generated. The contact area was calculated by a custom-developed image processing code that summed the area of black pixels (MATLAB®, Mathworks, Natick, Massachusetts, USA).

2.3. Statistical analyses

Statistical analyses compared the model to the experimental results. Three linear regression models were created to assess contributions from components of the multiscale model to the experimentally-measured ACOF. The first statistical analysis quantified the impact of COF predicted by the multiscale model on ACOF. The other statistical models quantified the ACOF predicted by 1. the shear stress predicted by the microscopic model at 200 kPa (roughly the average under-shoe contact pressure (Grönqvist, 1995)) and 2. the contact area from the macroscopic model. A linear regression model between the experimentally-measured contact area and the contact area predicted by the model was performed as an intermediate validation of the macroscopic simulations. Goodness of fit was assessed using the R^2 values in linear regression models. An alpha value of 0.05 was used for all statistical analyses.

Table 2
Shoe-floor angles in friction tests (Average(SD)).

Shoe	Shoe-Floor Angle-Vinyl (°)	Shoe-Floor Angle–Ceramic (°)
S1	6.43 (1.01)	6.90 (0.39)
S2	6.48 (0.38)	6.97 (0.13)
S3	6.21 (0.96)	7.53 (0.18)
S4	6.05 (0.78)	5.53 (0.43)
S5	7.79 (0.46)	6.40 (0.34)
S6	7.85 (0.49)	5.40 (0.59)
S7	7.32 (0.33)	7.27 (1.27)
S8	7.00 (0.22)	7.37 (1.32)

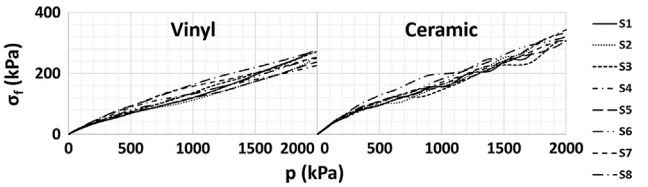

Fig. 3. Frictional shear stress, σ_f, as a function of contact pressure for different shoes when modeled against Vinyl (Left) and Ceramic (Right) flooring.

3. Results

The slopes of the piecewise polynomials (Eq. (3)) for relating σ_f values to contact pressure (Fig. 3) were generally higher at lower contact pressures. The shear stress, σ_f, was generally higher for ceramic flooring (higher roughness) compared to the vinyl flooring (lower roughness) (Fig. 3). For example, σ_f values at 200 kPa ranged between 34.1 and 43.6 kPa for vinyl flooring (Fig. 3. Left) and between 50.7 and 59.9 kPa for ceramic flooring (Fig. 3. Right).

The contact area geometry in the simulations were similar to the experimental contact geometries (Fig. 4). A strong correlation existed between predicted and measured contact areas (R^2 = 0.82; p = 0.002) (Fig. 5). Similar magnitudes were observed in the model-predicted contact areas (range of 1.44–9.29 cm^2) and the experimentally-measured contact areas (range of 2.02–11.83 cm^2).

The multiscale model predictions of COF (COF_{Model}) were correlated to the measured COF (ACOF) ($p < 0.001$, r = +0.86) and predicted 73% of the variance (Fig. 6). The magnitudes of the model predictions were lower than the experimental results. COF_{Model} had a narrower range (0.13–0.26) than the ACOF (range of 0.05–0.87). The slope of this regression line was 5.7. The shear stress of the microscopic model, predicted only 23 percent of the variation in ACOF (p = 0.059, r = +0.48). The contact area from the macroscopic model explained 34 percent of the variation in ACOF (p = 0.017, r = +0.58).

4. Discussion

The presented multiscale modeling predicted most of the variability for the experimentally-measured ACOF and contact area. Parameters from the microscale and macroscale components were

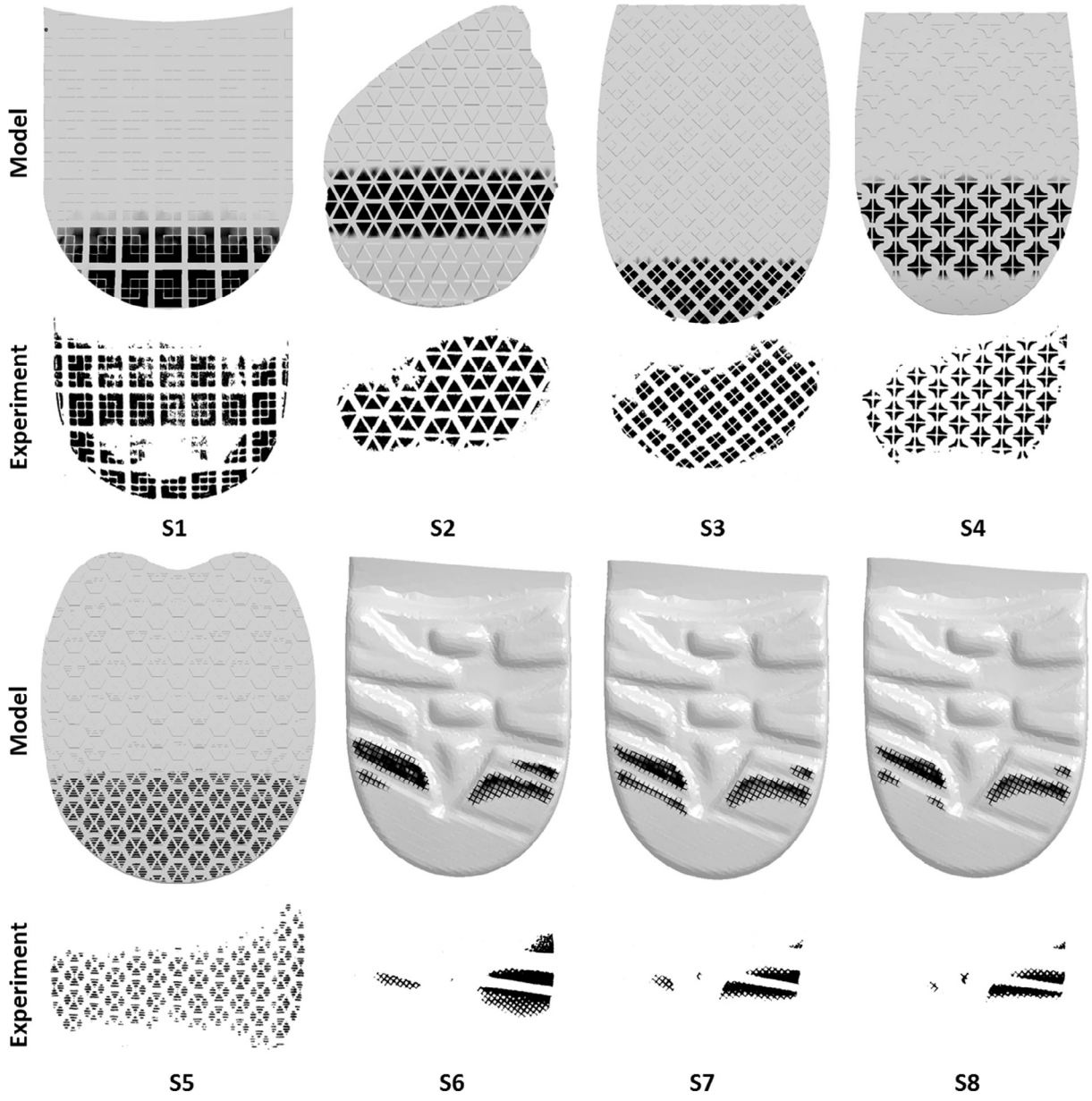

Fig. 4. Predicted macroscopic contact area and experimentally-measured contact area using the ink imprints. For the model, gray indicates no contact and black indicates contact. For the experiment, white indicates no contact and black indicates contact.

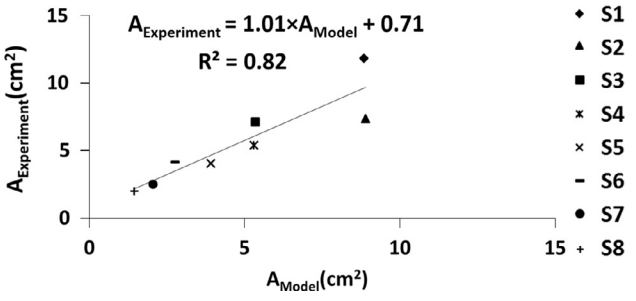

Fig. 5. Experimentally-measured contact area versus contact area predicted by the macroscopic model.

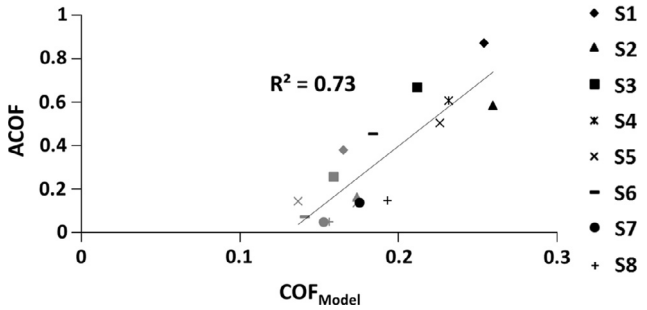

Fig. 6. Experimentally-measured ACOF versus COF predicted by the multiscale model. Marker colors represent floorings: vinyl (Gray) and ceramic (Black).

much less predictive of ACOF. This demonstrates the important contributions of each scale to successfully predict the whole shoe-floor ACOF.

The model predicted that shoe designs which lead to lower contact pressures will result in higher COFs and therefore lower the slip risk. This finding is consistent with computational modeling

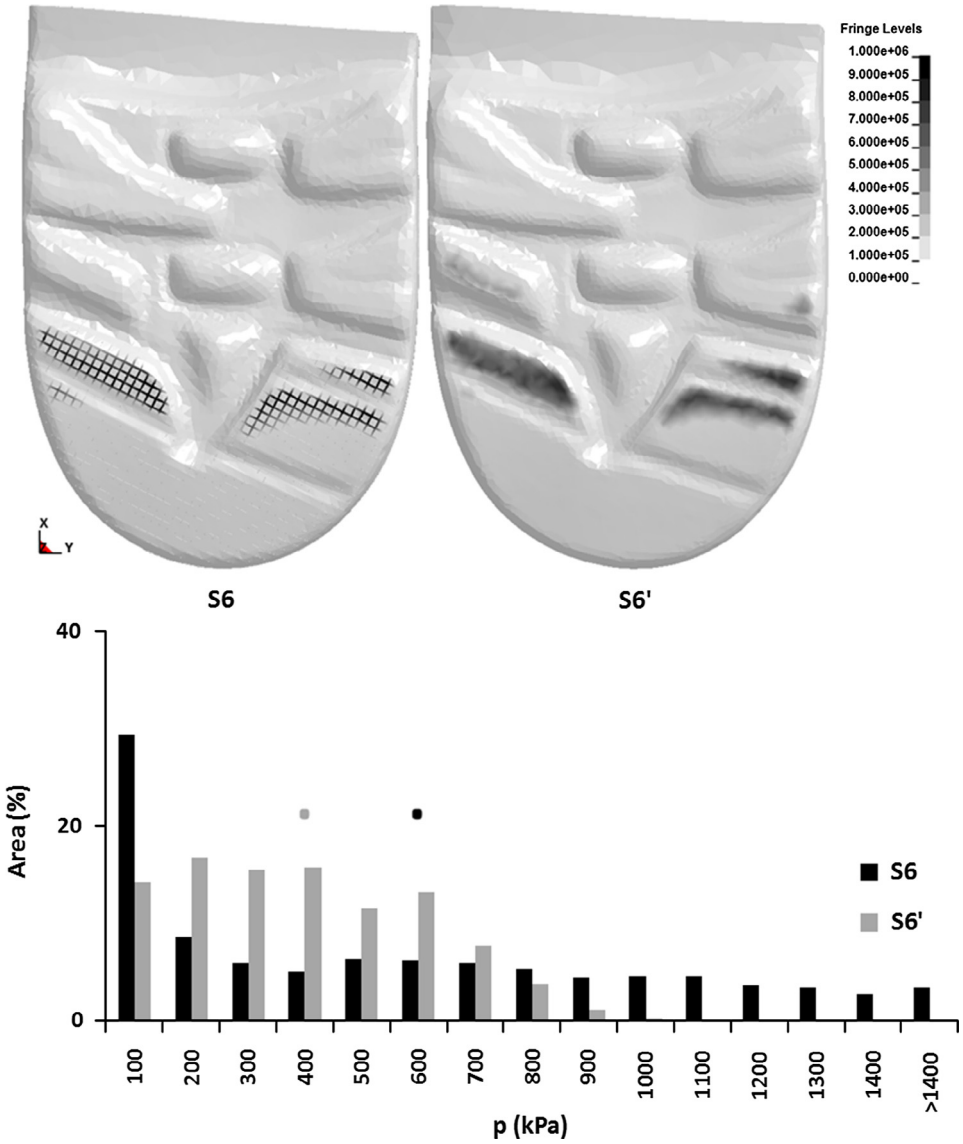

Fig. 7. Top: contact pressure distribution in a textured shoe (S6) versus the same shoe after removing the texture (S6′). Bottom: histogram of contact pressure distribution over the areas of a textured (S6-black) versus non-textured (S6′-gray) shoes. Circles indicate average contact pressures.

studies on rubber (Wagner et al., 2015b) and experimental findings of Grönqvist (Grönqvist, 1995) that reported lower COFs at higher contact pressures. The model also suggests that higher contact areas between shoe and flooring will result in higher COFs and lower fall risk in agreement with previous research (Chang and Matz, 2001; Grönqvist, 1995; Menz et al., 2001; Tencer et al., 2004). The microscopic model was sensitive to changes in floor roughness, consistent with experimental (Chang, 1998; Chang et al., 2001b) and modeling studies (Beschorner et al., 2009; Moghaddam et al., 2015). This increase in COF for rougher floor surfaces is due to larger viscoelastic deformation and energy loss (Grosch, 1963; Heinrich, 1997) in shoe material when it is subjected to floorings with higher asperity heights (high roughness floorings).

The outcomes of this research can be particularly useful in designing shoes by focusing on design characteristics that increase hysteresis COF. According to the model, a high COF on contaminated surfaces in boundary lubrication can be achieved by more distributed contact pressures. For example, the multiscale modeling framework can explain effects of tread texturing on COF. Overall, shoes with harder outsoles (S7 and S8) and texturing (S5-S8) demonstrated lower COFs compared to the other shoes. To demonstrate the impact of texture, another simulation was performed on S6 with the texturing removed (S6′). When tread texturing was removed (Fig. 7. Top), a lower average contact pressure (S6′) was observed (Fig. 7. Bottom). An increase in COF was observed on vinyl and ceramic flooring from 0.14 and 0.19 to 0.16 and 0.21, respectively. Based on the regression equation (Fig. 6) these changes in COF_{Model} would be expected to increase ACOF on vinyl and ceramic floorings by 0.12 and 0.17, respectively. This finding is consistent with some experimental literature that suggests the use of surface texturing for reducing friction in boundary lubrication (Pettersson and Jacobson, 2003, 2004) and with the shoe design recommendations that suggest that tread texturing would not always cause an improvement in footwear slip-resistance (Menz et al., 2001; Wilson, 1990). However, it should be noted that texturing can also lead to an increase in wet COF by preventing hydroplaning (Varenberg and Gorb, 2009). This study utilized treaded shoes which have been shown to operate in boundary lubrication (Beschorner et al., 2014; Singh and Beschorner, 2014). Thus, the surface texturing might have been unnecessary for fluid drainage, which may explain why an increase in COF was not observed.

Significant differences were observed between the COF magnitudes of the model predictions and the experimental data. However, these differences appear to scale linearly. The differences in COF magnitude could be due to modeling simplifications that deviate from the actual physics. For example, the model only considers hysteresis friction forces originating from the microscopic scale. However, hysteresis deformation and hysteresis friction can occur at multiple length scales from the nanometer scale to the millimeter scale. These forces are additive (Kluppel and Heinrich, 2000; Persson, 2001; Wagner et al., 2015b) and therefore increasing the number of scales used in the multiscale modeling would likely lead to larger overall predictions of hysteresis forces and hysteresis COF. Another simplifying assumption in the model is the uniform asperity heights. Real surfaces have a distribution of asperity heights, which causes the largest asperities to come into contact at lower contact pressures followed by asperities of lower heights coming into contact at higher contact pressures (Greenwood and Williamson, 1966). Because microscopic hysteresis friction is dependent on asperity height (Moghaddam et al., 2015), using probabilistic asperity height distributions for shoe and floor topography is likely to alter the frictional shear stress lines (Fig. 3) by changing the slope of those lines.

Notably, this study suggests that modeling on multiple scales improves the ability of the model to estimate shoe-floor COF. The current model using a simple 2-scale approach was able to capture much of the variability observed experimentally. While further refinements and potentially additional scales may increase the predictive capability, the present model might be sufficient when used along with a scaling factor (e.g. slope of the fit line in Fig. 6) to predict ACOF. As this model is extended to more shoe and flooring designs, it should become clearer whether more complexity or the scaling factor provides the best predictions.

Future improvements to the model may include more sophisticated material characterization and modeling adhesion forces and fluid pressures. For example, viscoelastic stress-relaxation testing similar to our previous work (Moghaddam et al., 2015), can be included. The current shoe-floor friction model did not consider the contributions due to adhesion. Thus, these findings may not apply to conditions where adhesion forces are substantial (dry or wet conditions with lower viscosity fluids). Future versions of this model may also include the impacts of the interfacial wear of the shoe outsole (Moghaddam et al., 2014) to predict COF in several stages of shoe life. Furthermore, the modeling introduced in this paper only examined the shoe-floor friction in one subset of testing conditions relevant to slip-testing. Future versions should examine the effect of different shoe-floor angles on the contact area and COF (Moghaddam and Beschorner, 2017) since it is expected that different shoe-floor angles lead to changes in contact area, COF and therefore slip risk (Moghaddam and Beschorner, 2017; Moyer et al., 2006).

The long-term goal of these computational models is to reduce slip and fall accidents by improving shoe and floor designs. Findings of the multiscale model presented here suggests that floor roughness, shoe contact area, and shoe tread design influence shoe-floor COF in lubricated conditions. These findings can be applied to optimize shoe and flooring designs to improve their slip-resistance performance and achieve the ultimate goal of reducing slips and falls accidents.

Funding

This work was supported by funding from that National Institute for Occupational Safety and Health (NIOSH R01 OH008986 and R01OH010940). Some of the footwear used in this study was provided by Timberland®.

Conflict of interest statement

The authors declare that they have no conflict of interest.

References

Aschan, C., Hirvonen, M., Mannelin, T., Rajamäki, E., 2005. Development and validation of a novel portable slip simulator. Appl. Ergon. 36, 585–593.
ASTM, 2010. D2240, Test Method for Rubber Property-Durometer Hardness. ASTM International.
ASTM, 2011. Standard Test Method for Measuring the Coefficient of Friction for Evaluation of Slip Performance of Footwear and Test Surfaces/Flooring Using a Whole Shoe Tester. ASTM International.
Beschorner, K., Lovell, M., Higgs III, C.F., Redfern, M.S., 2009. Modeling mixed-lubrication of a shoe-floor interface applied to a pin-on-disk apparatus. Tribol. Trans. 52, 560–568.
Beschorner, K.E., 2008. Development of a Computational Model for Shoe-Floor-Contaminant Friction. ProQuest.
Beschorner, K.E., Albert, D.L., Chambers, A.J., Redfern, M.S., 2014. Fluid pressures at the shoe–floor–contaminant interface during slips: effects of tread & implications on slip severity. J. Biomech. 47, 458–463.
Beschorner, K.E., Albert, D.L., Redfern, M.S., 2016. Required coefficient of friction during level walking is predictive of slipping. Gait Posture.
Beschorner, K.E., Redfern, M.S., Porter, W.L., Debski, R.E., 2007. Effects of slip testing parameters on measured coefficient of friction. Appl. Ergon. 38, 773–780.
Blanchette, M.G., Powers, C.M., 2015. The influence of footwear tread groove parameters on available friction. Appl. Ergon. 50, 237–241.
Burnfield, J.M., Powers, C.M., 2006. Prediction of slips: an evaluation of utilized coefficient of friction and available slip resistance. Ergonomics 49, 982–995.
Chang, W.-R., 1998. The effect of surface roughness on dynamic friction between neolite and quarry tile. Saf. Sci. 29, 89–105.
Chang, W.-R., Chang, C.-C., Matz, S., 2011. The effect of transverse shear force on the required coefficient of friction for level walking Human Factors. J. Human Fact. Ergon. Soc. 53, 461–473.
Chang, W.-R., Grönqvist, R., Hirvonen, M., Matz, S., 2004. The effect of surface waviness on friction between Neolite and quarry tiles. Ergonomics 47, 890–906.
Chang, W.-R., Grönqvist, R., Leclercq, S., Brungraber, R.J., Mattke, U., Strandberg, L., Thorpe, S.C., Myung, R., Makkonen, L., Courtney, T.K., 2001a. The role of friction in the measurement of slipperiness, part 2: survey of friction measurement devices. Ergonomics 44, 1233–1261.
Chang, W.-R., Kim, I.-J., Manning, D.P., Bunterngchit, Y., 2001b. The role of surface roughness in the measurement of slipperiness. Ergonomics 44, 1200–1216.
Chang, W.R., Matz, S., 2001. The slip resistance of common footwear materials measured with two slipmeters. Appl Ergon. 32, 549–558.
Courtney, T.K., Sorock, G.S., Manning, D.P., Collins, J.W., Holbein-Jenny, M.A., 2001. Occupational slip, trip, and fall-related injuries–can the contribution of slipperiness be isolated? Ergonomics 44, 1118–1137.
Cowap, M., Moghaddam, S., Menezes, P., Beschorner, K., 2015. Contributions of adhesion and hysteresis to coefficient of friction between shoe and floor surfaces: effects of floor roughness and sliding speed. Tribol.-Mater. Surf. Interfaces 9, 77–84.
Erhart, T., 2011. Review of Solid Element Formulations in LS-DYNA. LS-DYNA Entwicklerforum.
Florence, C., Haegerich, T., Simon, T., Zhou, C., Luo, F., 2015a. Estimated lifetime medical and work loss costs of fatal and nonfatal injuries, United States 2013. MMWR Morb. Mortal. Wkly. Rep. 64, 1074–1082.
Florence, C., Simon, T., Haegerich, T., Luo, F., Zhou, C., 2015b. Estimated lifetime medical and work-loss costs of fatal injuries-United States, 2013. MMWR. Morb. Mortal. Wkly. Rep. 64, 1074–1077.
Fortunato, G., Ciaravola, V., Furno, A., Scaraggi, M., Lorenz, B., Persson, B.N., 2017. Dependency of rubber friction on normal force or load: theory and experiment. Tire Sci. Technol. 45, 25–54.
Giacomin, A., Mix, A., 2011. Standardized polymer durometry. J. Testing Eval. 39, 1–10.
Goda, T., Year, On the Viscoelastic Component of Rubber Friction. In VI. InterNatl. Engineering Symposium at Banki, Budapest.
Greenwood, J., Williamson, J., Year, Contact of nominally flat surfaces. In: Proceedings of the Royal Society of London A: Mathematical, Physical and Engineering Sciences.
Grönqvist, R., 1995. Mechanisms of friction and assessment of slip resistance of new and used footwear soles on contaminated floors. Ergonomics 28, 224–241.
Grosch, K., Year, The relation between the friction and visco-elastic properties of rubber. In: Proceedings of the Royal Society of London A: Mathematical, Physical and Engineering Sciences.
Hanson, J.P., Redfern, M.S., Mazumdar, M., 1999. Predicting slips and falls considering required and available friction. Ergonomics 42, 1619–1633.
Heinrich, G., 1997. Hysteresis friction of sliding rubbers on rough and fractal surfaces. Rubb. Chem. Technol. 70, 1–14.
Hutchings, I., Shipway, P., 2017. Tribology: Friction and Wear of Engineering Materials. Butterworth-Heinemann.

Iraqi, A., Cham, R., Beschorner, K.E., 2015. Assessment of Slip-Risk using a Portable Slip Simulator. American Society of Biomechanics, Columbus, OH.
Kluppel, M., Heinrich, G., 2000. Rubber Friction on Self-Affine Road Tracks. Rubb. Chem. Technol. 73, 578–606.
Li, K.W., Chen, C.J., 2004. The effect of shoe soling tread groove width on the coefficient of friction with different sole materials, floors, and contaminants. Appl. Ergon. 35, 499–507.
Li, K.W., Wu, H.H., Lin, Y.-C., 2006. The effect of shoe sole tread groove depth on the friction coefficient with different tread groove widths, floors and contaminants. Appl. Ergon. 37, 743–748.
Menezes, P.L., Kailas, S.V., 2006. THE Role of Surface Texture on Friction and Transfer Layer Formation–A Study Of Aluminium and Steel Pair Using Pin-on-Plate Sldiing Tester.
Menz, H.B., Lord, S., McIntosh, A.S., 2001. Slip resistance of casual footwear: implications for falls in older adults. Gerontology 47, 145–149.
Moghaddam, S., 2013. Finite Element Analysis of Contribution of Adhesion and Hysteresis to Shoe-floor Friction.
Moghaddam, S., Iraqi, A., Beschorner, K., Year, Finite Element Model of Wear Progression in Shoe Soles. In: STLE Tribology Frontiers Conference.
Moghaddam, S.R.M., Beschorner, K.E., 2015. Multiscale Computational Modeling of Shoe-Floor Friction. American Society of Biomechanics, Columbus, OH.
Moghaddam, S.R.M., Beschorner, K.E., 2016. Multiscale Shoe-Floor Friction Model Predicts Impact of Shoe-Floor Angle on Utilized Coefficient of Friction During Slipping. American Society of Biomechanics, Raleigh, NC.
Moghaddam, S.R.M., Beschorner, K.E., Year, Sensitivity of a Multiscale Model of Shoe-Floor-Contaminant Friction to Normal Force and Shoe-Floor Contact Angle. In 2017 STLE Annual Meeting & Exhibition.
Moghaddam, S.R.M., Redfern, M.S., Beschorner, K.E., 2015. A microscopic finite element model of shoe-floor hysteresis and adhesion friction. Tribol. Lett. 59, 1–10.
Moore, C.T., Menezes, P.L., Lovell, M.R., Beschorner, K.E., 2012. Analysis of shoe friction during sliding against floor material: role of fluid contaminant. J. Tribol. 134, 041104.
Moyer, B., Chambers, A., Redfern, M.S., Cham, R., 2006. Gait parameters as predictors of slip severity in younger and older adults. Ergonomics 49, 329–343.
Persson, B., 2013. Sliding Friction: Physical Principles and Applications. Springer Science & Business Media.
Persson, B.N., 2001. Theory of rubber friction and contact mechanics. J. Chem. Phys. 115, 3840–3861.
Pettersson, U., Jacobson, S., 2003. Influence of surface texture on boundary lubricated sliding contacts. Tribol. Int. 36, 857–864.
Pettersson, U., Jacobson, S., 2004. Friction and wear properties of micro textured DLC coated surfaces in boundary lubricated sliding. Tribol. Lett. 17, 553–559.
Powers, C.M., Blanchette, M.G., 2014. Slip prediction accuracy and bias of the SATRA STM 603 whole shoe tester. J. Test. Eval. 43, 491–498.
Singh, G., Beschorner, K.E., 2014. A method for measuring fluid pressures in the shoe–floor–fluid interface: application to shoe tread evaluation. IIE Trans. Occup. Ergon. Human Fact. 2, 53–59.
Strobel, C.M., Menezes, P.L., Lovell, M.R., Beschorner, K.E., 2012. Analysis of the contribution of adhesion and hysteresis to shoe–floor lubricated friction in the boundary lubrication regime. Tribol. Lett. 47, 341–347.
Tabor D., 1974. Friction, Adhesion and Boundary Lubrication of Polymers. Advances in Polymer Friction and Wear. Springer, 5–30.
Tencer, A.F., Koepsell, T.D., Wolf, M.E., Frankenfeld, C.L., Buchner, D.M., Kukull, W.A., LaCroix, A.Z., Larson, E.B., Tautvydas, M., 2004. Biomechanical properties of shoes and risk of falls in older adults. J. Am. Geriatrics Soc. 52, 1840–1846.
Tsai, Y.J., Powers, C.M., 2008. The influence of footwear sole hardness on slip initiation in young adults. J. Forensic Sci. 53, 884–888.
Varenberg, M., Gorb, S.N., 2009. Hexagonal surface micropattern for dry and wet friction. Adv. Mater. 21, 483–486.
Wagner, P., Wriggers, P., Klapproth, C., Prange, C., 2015a. A Multiscale Contact Homogenization Approach for Hysteresis Friction of Rubber on Rough Surfaces. Book of Abstracts-Extract, 25.
Wagner, P., Wriggers, P., Klapproth, C., Prange, C., Wies, B., 2015b. Multiscale FEM approach for hysteresis friction of rubber on rough surfaces. Comput. Methods Appl. Mech. Eng. 296, 150–168.
Wilson, M.P., 1990. Development of SATRA Slip Test and Tread Pattern Design Guidelines, SLIPS, Stumbles, and Falls: Pedestrian Footwear and Surfaces. ASTM International.
Wriggers, P., Reinelt, J., 2009. Multi-scale approach for frictional contact of elastomers on rough rigid surfaces. Comput. Methods Appl. Mech. Eng. 198, 1996–2008.